EXPERIMENTAL STUDY ON ULTRASONIC WAVE PROPAGATION AND ATTENUATION CHARACTERISTICS IN HEAT EXCHANGERS

Yong WANG [1,2], Chang GAO [1,2], Guochun YAO [3], Yuhe SHANG [4,*]

[1]China Nuclear Power Operation Technology Corporation, Ltd., Wuhan Hubei, China

[2]Research Institute of Nuclear Power Operation, Wuhan Hubei, China

[3]School of Power and Mechanical Engineering, Wuhan University, Wuhan Hubei, China

[4]School of Energy and Mechanical Engineering, Nanjing Normal University, Nanjing Jiangsu, China

[*]Corresponding author; E-mail: yuhe_shang@163.com

The attenuation of ultrasonic wave propagation directly affects the descaling efficiency on the surface of heat exchangers. To investigate the attenuation characteristics of ultrasonic waves on the surface of heat exchangers, an experimental setup was designed and constructed, and the experimental measurements revealed the attenuation behavior of ultrasonic waves along the excitation direction, the horizontal direction, and the vertical direction. When ultrasonic waves propagate along the excitation direction, the sound intensity decays exponentially in front of the center of the barrel ($x < 50$ cm), which follows the theoretical value, while the sound intensity gradually increases behind the center ($x > 50$ cm). Horizontal to the propagation path in the excitation direction, the sound intensity varies less and is more stable. Furthermore, for a simplified heat exchanger model, the influence of the number of heat exchange tubes and their installation positions on the attenuation of ultrasonic wave propagation was thoroughly analyzed. The effect was found to be limited when the ratio of heat exchange tube to model diameter was $\leqslant$1/50 and the spacing was $\geqslant$0.195 m. Finally, a model for predicting the attenuation of ultrasonic sound intensity within the heat exchanger was proposed. This research provides valuable insights into the engineering application of ultrasonic descaling technology and the optimal design of heat exchangers.

Key words*: heat exchanger; ultrasonic wave; sound intensity; descaling*

1. Introduction

Under the dual background of global energy transition and the deep promotion of China's new industrialization, the demand for high-efficiency heat exchange equipment in key industrial fields such as electric power, chemical industry, and refrigeration continues to grow [1]. As the core component of energy conversion, the heat transfer efficiency of heat exchangers directly affects the system's energy consumption and operating costs [2]. However, during operation, particles in the water will continuously attach and accumulate on the surface of the heat exchanger, forming scale and increasing the thermal resistance, leading to a significant decrease in heat transfer efficiency (15%-30%), as well as

exacerbating the corrosion of the piping, which seriously affects the service life of the equipment and the operational efficiency [3].

To address this problem, although traditional chemical cleaning and mechanical descaling methods can solve the scale problem to a certain extent [4], there are problems such as environmental pollution and equipment damage [5]. In this context, ultrasonic descaling technology as a non-contact and environmentally friendly solution has received widespread attention [6]. The core mechanism lies in the cavitation and shear effects generated during the propagation of ultrasonic waves, which can effectively strip and inhibit scale formation [7]. However, it is worth noting that, in practical applications, ultrasonic propagation on the surface of the heat exchanger will be significantly attenuated, and this attenuation directly affects the energy distribution and descaling efficiency, which has become a key bottleneck in restricting the wide application of ultrasonic descaling technology [8].

Ultrasonic descaling technology has been extensively studied by researchers in several aspects [9]. Delouei et al. [10] showed that ultrasonic vibration destroys the boundary layer through acoustic cavitation and further enhances heat transfer by incorporating the dispersion of nanoparticles. On this basis, Hedeshi et al. [11] thoroughly investigated the synergistic effect of ultrasonic vibration with nanofluids, where uniform dispersion of nanofluids at low concentration has a synergistic effect with acoustic flow, and high concentration leads to increased deposition and pressure drop. In terms of frequency and power regulation, the systematic study by Gong et al. [12] shows that although high-frequency ultrasound (>100 kHz) can enhance the local cavitation intensity, its propagation distance is limited (<0.5 m), which makes it difficult to satisfy the coverage requirements of industrial-grade heat exchangers; whereas the low and mid-frequency bands (20-50 kHz) can achieve a larger range of homogeneous energy distribution due to better penetration properties. Echoing this, Wang et al.. [13] found that through the longitudinal wave velocity experiments of coal samples, the impact of material density differences on acoustic wave propagation is significantly stronger than the water content (a 5% reduction in density leads to a 6.6% decrease in velocity, while changes in water content caused only 2% fluctuations), which indirectly confirms the key role of medium density on acoustic wave attenuation. The effect of different material properties on ultrasonic attenuation has also been of interest [14], e.g., the acoustic impedance matching problem of stainless steel pipe walls exacerbates the reflection loss, while titanium alloys exhibit better acoustic energy transfer efficiency due to their low attenuation coefficients. Further explaining from the microscopic mechanism, Pippard et al. [15] revealed the quantization law of electron-phonon interaction on ultrasonic attenuation in metallic conductors: when the ultrasonic frequency reaches 10^9 Hz, the electron mean free range tends to be infinite, and at this time, the attenuation coefficient tends to be constant (about 0.15 dB/μm), which provides a microscopic scale basis for the design of the material suitability for the high-frequency ultrasonic waves. In addition, the position of the piezoelectric transducer will have an important effect on the ultrasonic waves, which needs to be dynamically adjusted according to the heat exchanger structure to maximize the cavitation effect and thermal boundary layer perturbation [16].

In summary, previous studies mainly focused on the optimization of ultrasonic parameters [17] (e.g., frequency, power), material acoustic properties, and nanofluid synergy effect [18], but insufficient attention was paid to the mechanism of the coupling effect between the structural parameters of the heat exchanger body and the spatial propagation paths of ultrasonic waves. For this reason, this study systematically investigates the attenuation characteristics of ultrasonic waves on the heat exchanger surface by combining experimental and theoretical analysis. A special experimental device is developed

to measure the attenuation of ultrasonic waves along the three propagation paths of excitation direction, horizontal direction, and vertical direction; based on the simplified heat exchanger model, the effects of structural parameters such as the number and spatial arrangement of heat exchanger tubes are quantitatively analyzed, and the correlation between geometrical configurations and attenuation modes is investigated to elucidate the regulatory mechanism of the number and position of tube bundles on the energy distribution of waves. In addition, a prediction model for the attenuation of ultrasonic sound intensity in the heat exchanger is proposed, which provides a quantitative tool for optimizing the descaling system.

2. Experimental Model

This section mainly introduces the experimental device for ultrasonic propagation attenuation measurement on the heat exchanger surface. As shown in Fig. 1(a), the experimental device consists of three parts: the ultrasonic excitation module, the heat exchanger body, and the acoustic signal acquisition system. Among them, the ultrasonic excitation module includes an ultrasonic generator and a magnetostrictive transducer: the generator dynamically regulates the amplitude with a center frequency of 10 kHz and an interval of 0.01 s. The transducer is driven to convert the electrical signal into mechanical vibration, and its high energy output characteristics (efficiency>85%) ensure a stable acoustic field required for descaling. The body of the heat exchanger is designed for the scaling down of the steam generator of the nuclear power plant, and the main body is a hollow cylindrical structure with a height of 1 m, an external diameter of 1 m, and a wall thickness of 0.005 m. The bottom is equipped with a stainless steel tube plate with a diameter of 1 m and a thickness of 0.05 m, and the surface is lined up with 11 holes according to the round shape, and the heat exchanger tubes are made of the same material with an external diameter of 0.019 m, a wall thickness of 0.002 m and a length of 1.1 m are arranged vertically on the surface. Acoustic signal acquisition system through the hydrophone (sensitivity-195 db) placed on the surface of the heat exchanger at a predetermined location to receive ultrasonic signals and convert them to electrical signals, and with the help of oscilloscopes to achieve real-time display of the waveforms and high-speed storage for attenuation characteristics of the analysis of the high-precision data to provide support. The device is shown in Fig. 1(b). The power of the ultrasonic transducer is 500 W, and the fluid in the heat exchanger is water.

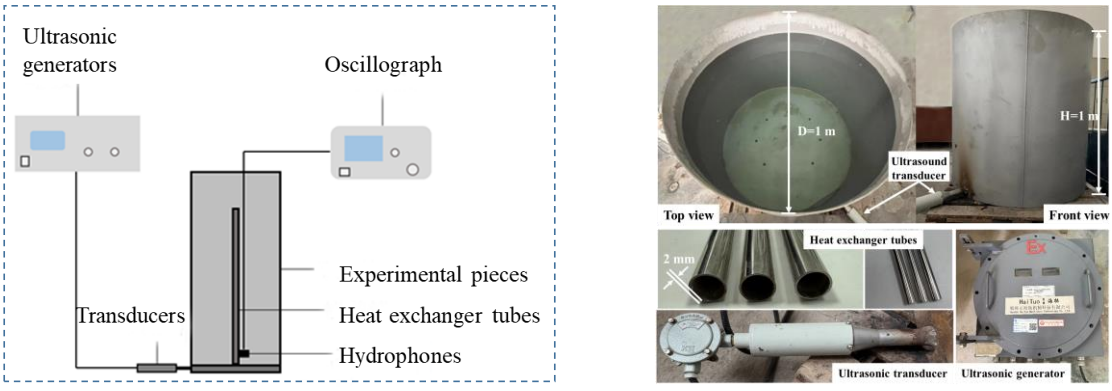

(a) (b)

Fig. 1 (a) Experimental schematic diagram of ultrasonic propagation attenuation characteristics. (b) Physical diagram of the experimental setup

3. Data Processing

3.1. Data Acquisition

To investigate the attenuation law of ultrasonic propagation on the heat exchanger surface, this study adopts the following experimental process to systematically investigate the attenuation characteristics of ultrasonic waves on the heat exchanger surface. First, in the data acquisition stage, the ultrasonic signal is measured at different locations on the heat exchanger surface by controlling the position movement of the hydrophone (Fig. 2), and 5 groups of acoustic pressure signals are repeatedly collected at each measurement point to reduce the random error. The ultrasonic signals were transmitted to a digital oscilloscope via a shielded cable to display the time domain waveforms in real-time and record parameters such as peak voltage, spectral energy distribution, etc. The data were synchronized and saved to an encrypted USB flash drive to prevent loss. In the data processing stage, a customized analysis program is developed based on the Python platform. Firstly, since the noise source mainly comes from mechanical vibration and electromagnetic noise, a filter function is used to eliminate environmental electromagnetic interference and mechanical vibration noise. Subsequently, based on the voltage sound intensity conversion formula, the voltage signal is converted to the effective sound pressure value, and then, the effective sound pressure at each position is calculated according to Eq. (1), and the sound intensity calculation formula is used to quantify the attenuation rate of the acoustic energy at each point. The scheme ensures that the data confidence level is over 95% through redundant measurements and multi-level calibration, which provides a reliable basis for the subsequent modeling of the attenuation law.

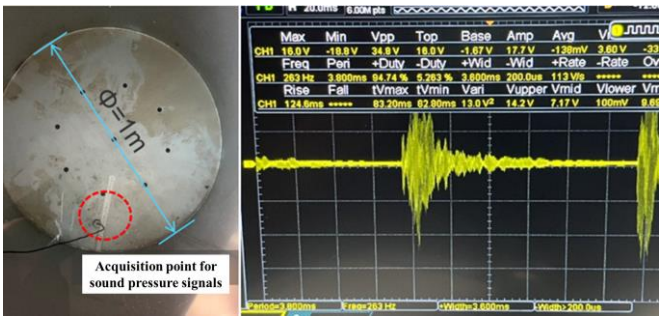

Fig. 2 Data acquisition

$$P = \sqrt{\frac{1}{N}\sum_{n=1}^{N} x^2(n)} \tag{1}$$

Where P represents the sound pressure (Pa), N denotes the number of time-domain sampling points, and $x(n)$ signifies the value of the time-domain sampling points.

3.2. Sound Intensity Calculation Method

The intensity of ultrasonic waves accurately reflects the energy strength of the ultrasonic signals, providing crucial support for subsequent data analysis and result interpretation. In this study, high-precision hydrophones were used to collect ultrasonic signals, which were displayed as open-circuit voltage on an oscilloscope. The ultrasonic intensity values were derived using Eq. (2). The free-field sound pressure at the hydrophone transducer was determined by the ratio of the open-circuit voltage to

the hydrophone sensitivity, as shown in Eq. (3). The hydrophone sensitivity was calculated based on its sensitivity level, with the calculation method outlined in Eq. (4). In these equations, I represents the ultra-sonic intensity (W/m²), P denotes the free field sound pressure (Pa), U is the open circuit voltage (V), M indicates the hydrophone sensitivity (V/Pa), M_0 is the reference value set at M_0=106 V/Pa, and H_M is the sensitivity level. The sensitivity level of the hydrophone used in this study is H_M=−190 dB.

$$I = \frac{P^2}{c\rho} \tag{2}$$

$$P = U / M \tag{3}$$

$$M = 10^{HM/20} M_0 \tag{4}$$

4. Results Analysis and Discussions

4.1. Study on Surface Ultrasonic Attenuation Characteristics of Simplified Heat Exchanger Model

4.1.1 Attenuation Characteristics of Ultrasonic Waves in the Direction of Excitation

In this section, we measured the variation of sound pressure along the excitation direction (i.e., the X direction) to investigate the propagation attenuation characteristics of ultrasound in that direction. Fig. 3(a) illustrates the measurements taken along the excitation direction. In the experiment, a hydrophone was used to collect data at 5 cm intervals, starting from the sound source excitation point, yielding a total of 20 measurements at different locations. Fig. 3(b) presents the specific measurement results of sound intensity along the excitation direction. In Fig. 3(b), the red curve represents the theoretical values calculated using Eq. (5)[19], and the black points with error bars indicate the experimental values and their error ranges. It is evident from Fig. 3(b) that within the heat exchanger and near the sound source excitation point (X = 0), the sound intensity reaches its peak at approximately 140 W/m². As the distance from the sound source increases, the sound pressure exhibits a fluctuating trend, yet overall, it adheres to the attenuation law. Notably, although the experimental values align well with the theoretical values at most points, significant deviations occur at certain specific locations. This deviation is particularly pronounced in the region where X > 50 cm. When the measurement point reaches X = 80 cm, the experimentally measured sound intensity is approximately 120 W/m². Overall, as ultrasound propagates within the heat exchanger along the excitation direction, the sound intensity demonstrates an exponential decay trend in the left half of the heat exchanger (i.e., X < 50 cm), maintaining good consistency with the theoretical calculations. However, once the ultrasound propagates into the right half of the heat exchanger (X > 50 cm), the sound intensity measurements begin to show an increasing trend. The enhancement of the sound intensity in the right half of the heat exchanger (X > 50 cm) can be explained by the following mechanisms: first, the solid boundary of the heat exchanger leads to multiple reflections of ultrasonic waves. In the region X > 50 cm, the phase difference between the incident and reflected waves creates phase-length interference, which triggers local energy superposition. Second, the heat exchanger forms a resonant cavity in the X > 50 cm region. When the ultrasonic frequency (10 kHz) is close to the intrinsic frequency in this region, standing wave formation leads to energy aggregation. Third, in the X > 50 cm region, longitudinal waves are partially

converted to shear waves at the wall interface. The converted shear wave has a lower attenuation rate ($\alpha_{\text{shear wave}} < \alpha_{\text{longitudinal wave}}$), which makes the energy propagation in this region more efficient. Regarding the energy source, the enhancement of sound intensity is not due to additional energy input, but rather to energy redistribution due to the above mechanism. The total energy of the system is conserved, and the energy loss in the left half (X < 50 cm) is partially offset by the energy recovery in the right half.

$$I = I_0 e^{-\alpha x} \tag{5}$$

$$\alpha = \frac{0.1 f^2}{1 + f^2} + \frac{40 f^2}{4100 + f^2} \tag{6}$$

In the Eq. (5) and Eq. (6), I represents the theoretical sound intensity (W/m²), I_0 denotes the sound intensity at the source of excitation (W/m²), α is the sound attenuation coefficient (dependent on the physicochemical properties of the working medium), f is the frequency of ultrasonic excitation (kHz), and x is the distance from the point of ultrasonic excitation (m).

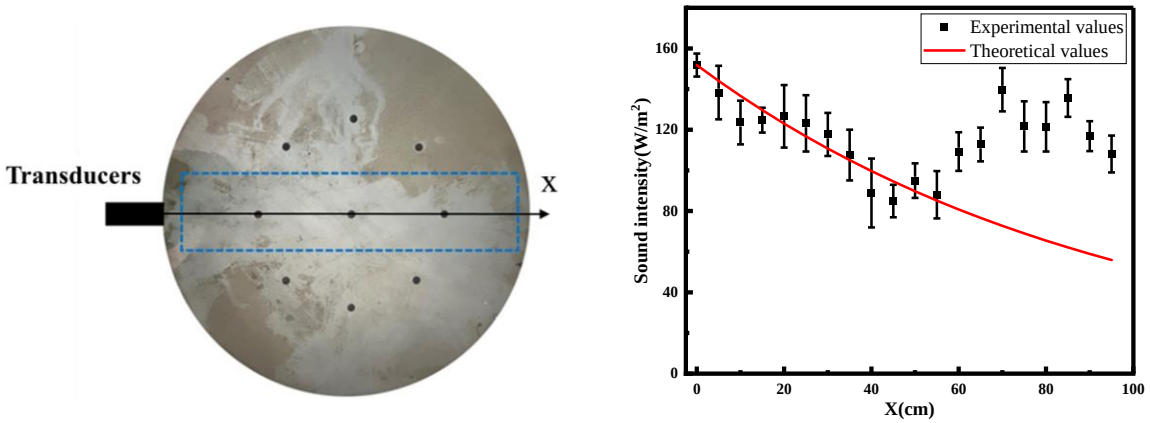

(a) (b)

Fig. 3 (a) Schematic diagram of the measurement along the direction of ultrasonic excitation. (b) The change in the sound intensity of the ultrasound wave along the direction of excitation

4.1.2 Attenuation Characteristics of Ultrasound Propagation in the Horizontal Direction Perpendicular to the Excitation Direction

In this section, we investigate the attenuation characteristics of ultrasound propagating horizontally, perpendicular to the excitation direction (i.e., along the Y-axis). To achieve this, experiments were conducted to measure the ultrasound sound pressure levels. Fig. 4(a) illustrates the positions of the measurements taken along the horizontal direction. During the experiment, a hydrophone was used as the measurement tool to collect data. A total of 20 distinct measurement points were selected along the Y-axis, with a 5 cm interval starting from the outermost edge of the central axis. Fig. 4(b) depicts the variation in sound intensity of the ultrasound along the horizontal direction perpendicular to the excitation. It is evident from Fig. 4(b) that the sound intensity of the ultrasound exhibits pronounced fluctuations in the horizontal direction perpendicular to the excitation. The sound intensity peaks at approximately 50 cm along the Y-axis, reaching nearly 140 W/m², indicating that the ultrasound energy is most concentrated at this position. Conversely, the lowest sound intensities are

observed at approximately 20 cm and 70 cm along the Y-axis, around 80 W/m², suggesting weaker ultrasound energy at these locations. Overall, the average sound intensity of the ultrasound along the horizontal direction perpendicular to the excitation is approximately 106 W/m², the standard deviation of the sound intensity values was 16.23 W/m², indicating significant dispersion in the data. In general, the sound intensity is relatively high in the central region of the heat exchanger, while it is comparatively lower near the sidewall regions. This distribution can be attributed to the propagation behavior of ultrasound in the far-field region, where the sound waves behave as spherical waves. In the central area, due to the proximity to the sound source, the propagation path of the sound waves is relatively short, resulting in higher sound intensity values. In contrast, near the walls, some sound waves are reflected or refracted upon encountering the walls, and these scattered and reflected waves interfere with the original sound field, leading to variations in the sound intensity values.

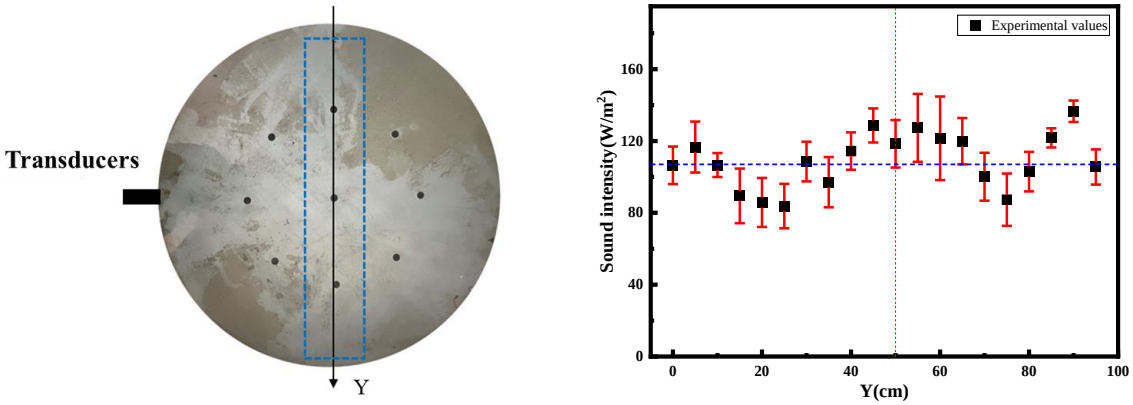

(a) (b)

Fig. 4 (a) Schematic diagram of measurement along the ultrasound horizontally and perpendicular to the direction of excitation. (b) The sound intensity of the ultrasound wave changes horizontally perpendicular to the direction of excitation

4.1.3 The Attenuation Law of Ultrasound Waves Along the Vertical and Perpendicular to the Excitation Direction

To construct a three-dimensional model of ultrasound wave attenuation during propagation in a heat exchanger, we explored the attenuation characteristics of ultrasound along the direction perpendicular to the excitation direction in the vertical plane (i.e., the Z-axis). Sound pressure values of the ultrasonic signals were measured at 5 cm intervals, yielding a total of 20 data points at different locations. Fig. 5(a) illustrates the spatial distribution of the measurement locations. As shown in Fig. 5(a), the experiment focused on three different positions: near the tube wall (labeled as Z_3), at the center (labeled as Z_1), and at an intermediate position between the wall and the center (labeled as Z_2). This approach provided a comprehensive understanding of ultrasonic wave propagation at different spatial locations. Fig. 5(b) demonstrates the attenuation of ultrasonic waves along the Z_1, Z_2, and Z_3 axes. It can be observed that, with a fixed position along the X-axis, the sound intensity shows a clear decreasing trend as the measurement height increases. At position Z_3, the sound pressure intensity dropped from nearly 100 W/m² to approximately 50 W/m². At position Z_2, the variation range was smaller but still showed a distinct decreasing trend. At position Z_1, the decrease was even more pronounced, from about 60 W/m² to nearly 10 W/m². This behavior can be attributed to the far-field propagation of ultrasonic

waves as spherical waves, where energy disperses and attenuates with increasing distance from the source, leading to a corresponding reduction in sound intensity. Additionally, at a fixed vertical height (constant Z-coordinate), sound intensity increases as the horizontal distance to the sound source decreases. This indicates that in the region near the sound source, the sound intensity can be maintained at a relatively high level due to the lower attenuation of the ultrasound waves. This finding further supports the strong relationship between ultrasonic wave attenuation and distance during propagation. To systematically quantify the attenuation characteristics of ultrasonic sound intensity in the vertical direction (Z-axis), data fitting techniques were employed [20], yielding a corresponding fitting equation (Eq. (7)). The exponential decay model was chosen [21], because it is widely accepted in acoustics for describing attenuation in homogeneous media [22], due to mechanisms like absorption and scattering. Local fluctuations in experimental data may be caused by the following factors: medium inhomogeneity (e.g., microscopic impurities in liquids), measurement errors (e.g., sensor coupling effects, environmental noise interference), or near-field effects (e.g., superposition of reflected waves over short distances). However, the overall trend aligns with the exponential decay model, and after statistical averaging (averaging multiple measurements), the data still exhibits a high degree of agreement with the model (R^2), with all values exceeding 0.79. The mean absolute percentage error (MAPE) between the measured data and the theoretical model was 7.8%, which verified the reliability of the model in predicting the sound field distribution in the vertical direction. This equation can serve as a predictive model for the attenuation of ultrasonic waves propagating vertically perpendicular to the excitation direction within the heat exchanger.

$$I_Z = I_{Z,0} e^{-\alpha z} \tag{7}$$

In the equation, α_1 = 0.01162, α_2 = 0.00792, α_3 = 0.00720 correspond to the fitting parameters for positions Z_1, Z_2, and Z_3, respectively.

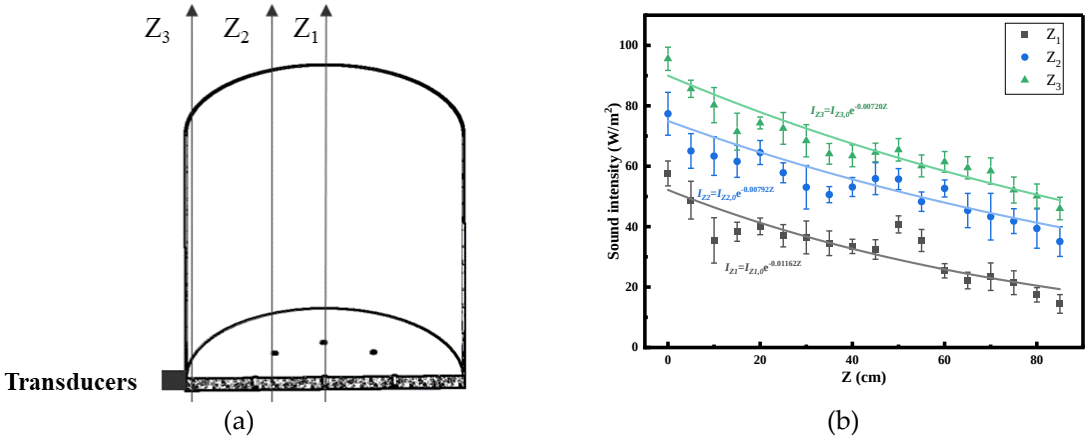

Fig. 5 (a) Schematic diagram of the measurement along the height direction. (b) The sound intensity of the ultrasound wave changes vertically perpendicular to the direction of excitation

4.2. The Influence of the Position and Quantity of Heat Exchange Tubes on Ultrasonic Attenuation

In this section, we investigated the impact of heat exchange tube layout (placement and quantity) on ultrasonic wave attenuation. Fig. 6 provides a detailed depiction of the configuration of heat exchange tubes inside the heat exchanger and the specific arrangement of sound intensity measurement points.

The heat exchange tubes are placed at eight distinct positions, numbered from Position 1 to Position 8. To explore the attenuation pattern of ultrasonic waves in the vertical direction, sound intensity measurements were conducted at four different vertical heights (Z = 0 m, 0.1 m, 0.5 m, 0.7 m) at the center of the heat exchanger. Fig. 7(a) illustrates the distribution of sound intensity across these positions at the specified heights. The sound intensity appears independent of the measurement location due to the complex sound propagation characteristics in the x-direction. In conjunction with Fig. 3(b), the sound intensity initially decays by 40% from 150 W/m² to 89 W/m² over 0-40 cm and then increases by 57% to 140 W/m² at 75 cm. This "attenuation-enhancement" phenomenon is caused by the superposition of reflected waves from the heat exchanger tubes and standing waves near the tube bundle. Thus, despite the spatial separation between measurement points 1 (25 cm) and 5 (75 cm), similar sound intensities are observed due to wave interference. In addition, the propagation of sound intensity in the vertical direction is notably affected by height, with sound intensity gradually decreasing as height increases. At the lowest height (Z = 0 m), sound intensity reaches its maximum value, fluctuating between 60 and 70 W/m², indicating the strongest intensity near the excitation source. At Z = 0.1 m, the sound intensity slightly decreases, remaining within the range of 60 to 65 W/m². As the height increases to Z = 0.5 m, the intensity further reduces to approximately 50 W/m². By Z = 0.7 m, the sound intensity significantly diminishes to about 30 W/m². Experimental results indicate that while there were some variations in the specific values of sound intensity, these variations were not significant enough to establish a clear position-dependent trend. The overall sound intensity appeared independent of the measurement location due to the complex interference patterns caused by reflected and standing waves. The direct impact of tube placement on ultrasonic attenuation is relatively small. Different heat exchange tubes were installed to investigate the effect of the number of heat exchange tubes on the propagation and attenuation of ultrasonic waves in the heat exchanger, and sound intensity measurements were taken. Fig. 7(b) demonstrates the impact of the number of tubes on ultrasonic wave propagation and attenuation. From the figure, it is evident that the fluctuation in sound intensity is not significant as the number of heat exchange tubes increases. As the number of heat exchange tubes increases from 1 to 8, the variation range of sound intensity fluctuates between 60 and 70 W/m² without a significant decreasing or increasing trend. The above experimental results show that in the simplified heat exchanger model of this paper, when the ratio of the diameter of the heat exchange tube to the heat exchanger model is not greater than 1/50, and the spacing of the heat exchange tubes is not less than 0.195 m, the influence of the placement position and number of the heat exchange tubes on the attenuation of the ultrasonic wave propagation is very limited.

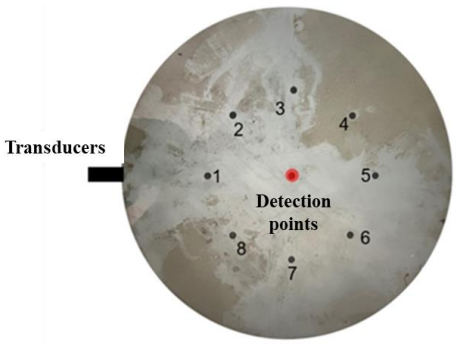

Fig. 6 Schematic diagram of the heat exchange tube placement

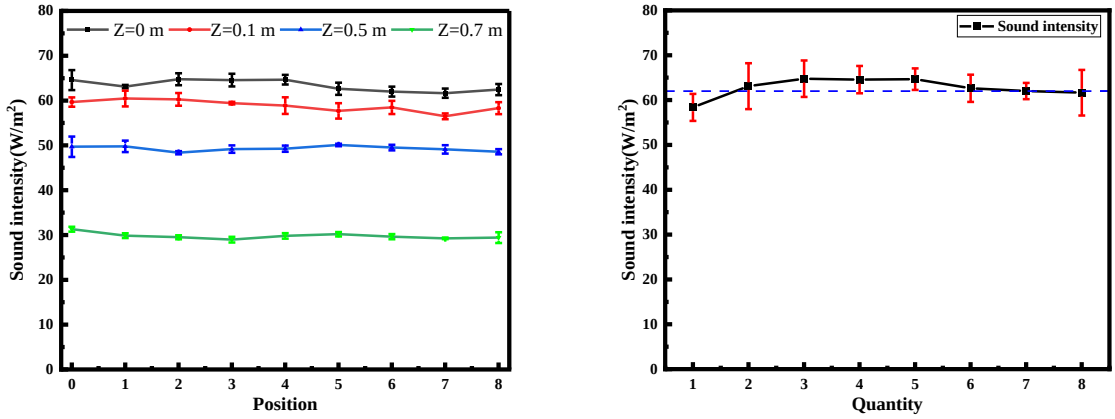

(a) (b)

Fig. 7 (a) The effect of the position of the heat exchange tube on the sound intensity of the ultrasonic wave. (b) The effect of the number of heat exchange tubes placed on the ultrasonic sound intensity

In this study, although some acoustic wave transmission laws were obtained in the experimental design and analysis, there are still deficiencies. The experimental model adopts a reduced design with a simple tube bundle arrangement, which can simulate the acoustic scattering, but it does not take into account the dense tube bundle vibration coupled with the acoustic field due to the turbulent excitation in the industry, which may bias the assessment of the acoustic attenuation intensity under the dynamic working condition. In addition, the study mainly focused on clean surfaces and did not investigate the dynamic effects of porosity changes in the fouling layer on the acoustic transmittance. In the future, we plan to develop a tube bundle-multiphase flow coupled acoustic transmission model, construct a digital twin platform, and dynamically simulate the scale growth and acoustic attenuation in real-time, as well as carry out full-size steam generator prototype experiments to further validate the vibration-medium multifactorial coupling effect, improve the research system, and enhance the applicability of the results.

5. Conclusions

In this study, we experimentally investigated ultrasonic attenuation inside a heat exchanger and examined the propagation and attenuation characteristics of ultrasonic waves influenced by the layout of heat exchange tubes. The attenuation and propagation characteristics of ultrasonic waves in different directions are summarized as follows:

(1) Excitation Direction (X-axis): When ultrasonic waves propagate inside the heat exchanger along the excitation direction, the sound intensity in the central region of the heat exchanger exhibits an exponential decay trend in the front half (X < 50 cm), closely aligning with theoretical calculations. In the rear half of the heat exchanger (X > 50 cm), the measured sound intensity gradually increases due to partial reflection and refraction of sound waves when they encounter the walls.

(2) Horizontal Propagation (Y-axis): Along the horizontal propagation path perpendicular to the excitation direction, the sound intensity exhibits noticeable fluctuations, with an average value of about 106 W/m². Minor variations in sound intensity are likely influenced by scattering and reflection during ultrasonic wave propagation, with a slight increase observed near the wall.

(3) Vertical Propagation (Z-axis): In the vertical propagation path perpendicular to the excitation direction, the variation in sound intensity is closely related to the spherical wave propagation

characteristics. At a fixed horizontal position, the sound intensity shows a clear decreasing trend as the measurement height increases. Conversely, at a fixed vertical height, the sound intensity increases as the horizontal distance to the sound source decreases.

(4) Heat Exchange Tube Layout: In the simplified heat exchanger model constructed in this study, different arrangements of heat exchange tubes resulted in sound intensity variations ranging from 60 to 70 W/m², without significant trends of increase or decrease. This suggests that the placement and number of heat exchange tubes in this study have a relatively minor direct impact on ultrasonic attenuation due to the complex interference patterns caused by reflected and standing waves.

Based on the findings, a predictive model for ultrasonic sound intensity attenuation within heat exchangers is proposed. This model accurately describes the propagation and attenuation characteristics of ultrasonic waves inside the heat exchanger, providing theoretical support for understanding ultrasonic wave propagation mechanisms. The research has significant implications for optimizing heat exchanger design and advancing the engineering application of ultrasonic descaling technology.

Acknowledgment

This research was funded by the Applied Basic Research Fund of the Hubei Nuclear Power Operation Engineering Technology Research Center.

Nomenclature

General symbols			
c	sound velocity (m/s)	M	hydrophone sensitivity (V/Pa)
f	frequency of ultrasonic excitation (kHz)	P	sound pressure (Pa)
H_M	sensitivity level	U	open-circuit voltage (V)
I	ultrasonic intensity (W/m²)	x	distance from the point of ultrasonic excitation (m)
Greek letters			
α	sound attenuation coefficient	ρ	density (kg/m^3)

References

[1] Xu, Y., *et al.*, Experimental study on the heat transfer performance of a phase change material based pin-fin heat sink for heat dissipation in airborne equipment under hypergravity, *Journal of Energy Storage*, *52* (2022), 104742

[2] Rezaei, P., *et al.*, Design and optimization of a spiral-tube instantaneous water heater using response surface methodology, *Water*, *15* (2023), 8, 1458

[3] Cheng, C., Yang, N., Multi-objective particle swarm optimization algorithm for data acquisition and system characteristics research of phase change thermal storage heat pump water heaters, *Thermal Science*, *28* (2024), 2B, pp. 1469-1476

[4] Jana, S., Subramanian, V. K., Formation and characterization of calcium carbonate scale on copper and aluminium substrates: Influence of chemical additives and heating methods at 60°C with application, *Surfaces and Interfaces*, *62* (2025), 106170

[5] Hasan, M. R., *et al.*, Efficacy of ultrasonic cleaning on cockle shells, *Journal of Food Engineering*, *352* (2023), 111523

[6] Amiri, D. A., *et al*., An active approach to heat transfer enhancement in indirect heaters of city gate stations: An experimental modeling, *Applied Thermal Engineering*, *237* (2024), 121795
[7] Amiri, D. A., *et al*., Louvered fin-and-flat tube compact heat exchanger under ultrasonic excitation, *Fire*, *6* (2022), 1, 13
[8] Luo, Y., *et al*., Study on scale formation and corrosion behavior of heat exchanger steel 20 at different temperatures, *International Journal of Electrochemical Science*, *19* (2024), 3, 100510
[9] Qu, Z., *et al*., Methodology for removing fouling within liquid-filled pipelines based on ultrasonic guided waves cavitation effect, *Applied Acoustics*, *157* (2020), 107018
[10] Amiri, D. A., *et al*.,The thermal effects of multi-walled carbon nanotube concentration on an ultrasonic vibrating finned tube heat exchanger, *International Communications in Heat and Mass Transfer*, *135* (2022), 106098
[11] Hedeshi, M., *et al*., Nanofluid as the working fluid of an ultrasonic-assisted double-pipe counter-flow heat exchanger, *Journal of Thermal Analysis and Calorimetry*, *148* (2023), 16, pp. 8579-8591
[12] Gong, T., *et al.*, Numerical study of cavitation shock wave emission in the thin liquid layer by power ultrasonic vibratory machining, *Scientific Reports*, *14* (2024), 1, 16956
[13] Wang, G., *et al.*, Experimental research on propagation and attenuation of ultrasonic waves in water-bearing coal, *Fuel*, *324* (2022), 124533
[14] Ono, K., A comprehensive report on ultrasonic attenuation of engineering materials, including metals, ceramics, polymers, fiber-reinforced composites, wood, and rocks, *Applied Sciences*, *10* (2020), 7, 2230
[15] Pippard, A. B., Theory of ultrasonic attenuation in metals and magneto-acoustic oscillations, *Proceedings of the Royal Society of London. Series A. Mathematical and Physical Sciences*, *257* (1960), 1289, pp. 165-193
[16] Delouei, A. A. , *et al.*, The effect of piezoelectric transducer location on heat transfer enhancement of an ultrasonic-assisted liquid-cooled CPU radiator, *Iranian Journal of Science and Technology, Transactions of Mechanical Engineering*, *48* (2024), 1, pp. 239-252
[17] Tafarroj, M. M. , *et al.*, MLP and optimized FCM-ANFIS models proposed for inlet turbulent flow under ultrasonic vibration, *Journal of Thermal Analysis and Calorimetry*, *148* (2023), 24, pp. 13995-14009
[18] Li, Y. , *et al.*, The modulation of response caused by the fractional derivative in the duffing system under super-harmonic resonance, *Thermal Science*, *25* (2021), 3B, pp. 2357-2367
[19] Thorp, W. H., Analytic description of the low-frequency attenuation coefficient, *The Journal of the Acoustical Society of America*, *42* (1967), 1, pp. 270-270
[20] Li, M., *et al*., Study of acoustic emission propagation characteristics and energy attenuation of surface transverse wave and internal longitudinal wave of wood, *Wood Science and Technology*, *55* (2021), 6, pp. 1619-1637
[21] Kon, T., *et al.*, Propagation characteristics of acoustic emission waves in liquid media in near-field, *Precision Engineering*, *77* (2022), pp. 220-226
[22] Hou, J., *et al.*, Study on propagation mechanism and attenuation law of acoustic emission waves for damage of prestressed steel strands, *Measurement*, *219* (2023), 113240

Received: 13.03.2025.
Revised: 16.06.2025.
Accepted: 24.06.2025.